THE JOURNAL OF PHYSICAL CHEMISTRY C

ARTICLE

pubs.acs.org/JPCC

Influence of Interface Morphology onto the Photovoltaic Properties of Nanopatterned ZnO/Poly(3-hexylthiophene) Hybrid Solar Cells. An Impedance Spectroscopy Study

Bert Conings,*[,†] Linny Baeten,[†] Hans-Gerd Boyen,[†] Donato Spoltore,[†] Jan D'Haen,[†,‡] Lars Grieten,[†] Patrick Wagner,[†,‡] Marlies K. Van Bael,[†,‡] and Jean V. Manca[†,‡]

[†]Institute for Materials Research, Wetenschapspark 1, B-3590 Diepenbeek, Belgium

[‡]Imec vzw Division IMOMEC, Wetenschapspark 1, B-3590 Diepenbeek, Belgium

Supporting Information

ABSTRACT: This paper focuses on the characterization of the ZnO/poly(3-hexylthiophene) (P3HT) interfaces in nanostructured hybrid solar cells, aiming to elucidate the relationship between thermal treatment, local morphology, and device performance. An equivalent impedimetric model for the device is proposed, allowing us to extract information about the ZnO/P3HT interface morphology and its impact on the photovoltaic properties by comparing devices with and without nanopatterning. It is found that the influence of thermal treatment on performance lies solely in the interface, resulting from a different interfacial morphology of P3HT depending on which crystal direction of ZnO is present.

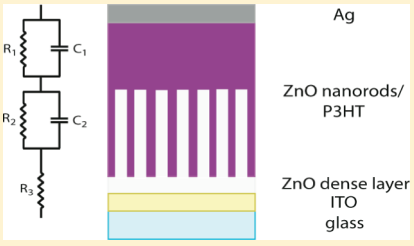

INTRODUCTION

In current generation organic and hybrid solar cells, the bulk heterojunction (BHJ) concept is by far the most successful one.[1−5] It consists of a network of two interpenetrating phases of which typically one absorbs light and transports hole-like carriers while the other transports electrons. One of the key issues on the way to efficient BHJ photovoltaic cells is thus to gain control over the morphology of both phases and their degree of phase separation.[6−8] On the one hand, the nanoscale domain size should not exceed the exciton diffusion length in the light absorber, as part of the excitons would be lost due to recombination prior to reaching an interface for charge separation. On the other hand, an excessively small domain size would impair charge transport to the electrodes. The big challenge thus remains to harvest as much light as possible without harming charge percolation.[9−11] In that respect, vertically aligned nanostructures are well accepted to offer a great potential in the development of next-generation hybrid solar cells. A large donor−acceptor interface area is guaranteed through the high density of nanostructures and, equally important, a direct pathway toward the electrodes after exciton dissociation is assured (in contrast to BHJs). Several types of nanorod arrays (predominatly ZnO and TiO_2) have been successfully used in different types of solar cells, ranging from liquid dye-sensitized solar cells to solid-state hybrids.[12−17] Although the highest efficiencies so far were obtained with TiO_2, the potential of ZnO cannot be overlooked. First of all, hydrothermal synthesis of single-crystalline ZnO nanorods allows for straightforward and low-cost production.[18,19] Moreover, ZnO has a higher electron mobility than TiO_2 and it is easier to finetune its morphology.[20−23]

However, TiO_2-based photovoltaics are currently well ahead of ZnO-based ones because the interfaces between the metal oxide and the electron donors are still less understood and, thus, not optimized yet in the latter case.[24,25] At any interface in a solar cell, physical and electrical phenomena largely influence the overall performance of the device at hand and, herein, the donor−acceptor interface is the most critical one. As excitons are split close to that interface, the local morphology of the dye or polymer in the vicinity of the metal oxide is crucial for the device properties and, when optimized, can drastically increase the efficiency.[25−29]

To gain more insight into the different components and interfaces in complex hybrid structures, impedance spectroscopy is a popular technique. Its power results from its ability to separate events that occur at different time scales or rates, which can be exploited to isolate diffusion and recombination processes.[30,31] Traditionally, it has been used in dye-sensitized solar cells and, more recently, in organic solar cells and hybrid structures as well.[32−39] Elaborate theoretical understanding of the technique for solar cell applications is aptly described.[31,33]

For solid-state hybrid solar cells, a particular difficulty is that the light-absorbing polymer has to be infiltrated into the already synthesized nanorod array.[28,40] In the case of P3HT as the absorber material, solvent annealing and thermal annealing have

Received: April 20, 2011
Revised: July 20, 2011
Published: July 22, 2011

been proposed to ensure full infiltration, where the latter one is the most effective so far.[17,28,41] In this contribution, impedance spectroscopy will be applied to study hybrid solar cells based on ZnO nanorod arrays and P3HT, thereby focusing on interface properties and their relation with device performance upon thermal treatment. Furthermore, charge extraction in a linearly increasing voltage (CELIV) is performed as a complementary technique to obtain additional information about the charge carrier mobility of P3HT as used in devices with and without nanopatterning.

MATERIALS AND METHODS

ZnO Nanorod Synthesis. ZnO nanorods were synthesized as described earlier using a two-step process consisting of seeding and hydrothermal growth.[17] Briefly, the seed layer was deposited by an aqueous sol−gel method onto patterned ITO (15 Ω/sq, Every Rich Enterprise Limited). To improve the wettability of the substrate for the aqueous precursor solution, the wet cleaning was followed by a 15 min UV−ozone treatment before spin coating. Next, the substrates were thermally treated to obtain a thin ZnO film of 20 nm. To vary the seed layer thickness up to 140 nm, the latter steps were repeated a number of times. The hydrothermal growth was executed at 95 °C for different times, depending on the desired nanorod length, in an equimolar aqueous solution of zinc acetate dihydrate (Aldrich) and hexamethylenetetramine (Aldrich) in deionized water. Afterward, the solution was cooled naturally for 1 h before the samples were removed. The samples were then rinsed with deionized water and dried at 60 °C for 1 h.

Photovoltaic Devices. The freshly prepared ZnO coated ITO substrates were heated at 150 °C for 20 min in air and cooled with N_2 flow prior to spin-coating low molecular weight P3HT (Rieke Metals) solutions in chlorobenzene (Aldrich).[28] After deposition, the samples were annealed at the melting temperature of P3HT (225 °C) in N_2 for different times to enhance infiltration into the nanorods and to enhance the crystallinity of the P3HT.[17] Finally, 80 nm Ag top electrodes were evaporated in vacuum (1×10^{-6} mbar).

Solar Cell Characterization. *IV* characterization was performed in air at room temperature, under an AM1.5 illumination of 100 mW/cm^2 with a Newport Oriel Class A model 91195A solar simulator. Impedance spectra (100 Hz to 5 MHz) were obtained using a HP 4194A Impedance/gain-phase analyzer, all in dark, with an oscillating voltage of 25 mV. The spectra were analyzed with ZSimpWin software (version 3.1, Princeton Applied Research). CELIV measurements were carried out by applying a ramp voltage on the sample (supplied by a function generator (Tektronix AFG 3101)) and monitoring the current transient response using a digital oscilloscope (Tektronix TDS 620B). The ramp amplitude was varied, which allows us to extract the charge carrier mobility as a function of electric field.[42]

RESULTS AND DISCUSSION

Recently, we reported on the influence of thermal treatment during the fabrication of ZnO nanorod/P3HT hybrid solar cells on their photovoltaic efficiency.[17] It was discovered that heating the polymer above its melting temperature (T_m = 225 °C) for 1 min enables it to fully infiltrate the nanorod array. Annealing considerably longer than 1 min was found to deteriorate the device performance severely. Because UV/vis measurements did not show any change in the optical properties of the polymer upon melting treatment, the decreasing device performance was attributed to the specific alignment of the polymer chains on top of the nanorods as discussed by Dag and coworkers,[43] thereby impeding charge transfer in the vertical direction. To study the interface between P3HT and ZnO in more detail, impedance spectroscopy is applied to ZnO/P3HT hybrid solar cells comprising either ZnO nanorods (NR) or ZnO dense layers (DL), the latter representing the reference system without nanopatterning.

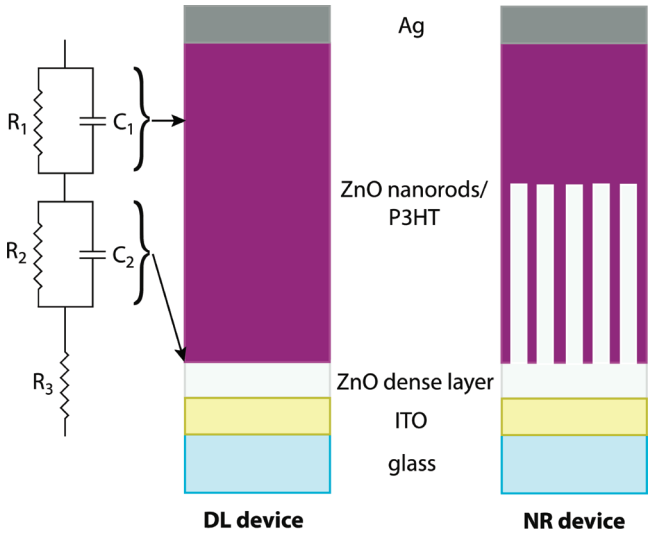

Figure 1. Experimental setup of a dense layer device (DL) and a nanorod device (NR), together with the proposed impedimetric model.

The basic setup of the different sample architectures (DL, NR) is sketched in Figure 1 together with the equivalent circuit model used to analyze the experimental data. Briefly, an ITO base electrode is covered by a dense ZnO film used as a hole blocking layer, followed either by a ZnO nanorod array filled with P3HT as the photoactive layer plus an additional P3HT layer used as electron blocking layer (NR device) or just by a pure P3HT film (DL device). In both cases, a thin Ag top electrode terminates the photovoltaic device.

To better understand the fundamental contributions to an impedance spectrum arising from specific parts of our device architecture, measurements were performed first on devices without nanostructuring. Figure 2a shows the Nyquist plot of a series of spectra acquired on a DL device for different bias voltages (full symbols). Despite the presence of four different materials (ITO, ZnO, P3HT, and Ag) and three interfaces (ITO/ZnO, ZnO/P3HT, and P3HT/Ag), the spectra only contain two main features: two semicircles with the left one revealing a small offset on the real axis. These spectra can be analyzed according to the model proposed in Figure 1, thereby assuming two parallel combinations of resistors and capacitors (C_1−R_1 and C_2−R_2 representing the two semicircles) in series with a resistor R_3 reflecting the observed small offset. The capacitors are treated as constant phase elements (CPE), which allows us to obtain better fits.[30,44,45] A CPE's impedance is defined as a complex number $Z = Q^{-1}(i\omega)^{-n}$, with Q representing a constant, ω the angular frequency, and n a number between 1 (ideal capacitor) and 0 (pure resistor). A CPE is, in fact, a generalized imperfect capacitance that takes into account surface roughness and heterogeneities.[30,44] In our case, extracted n values were most

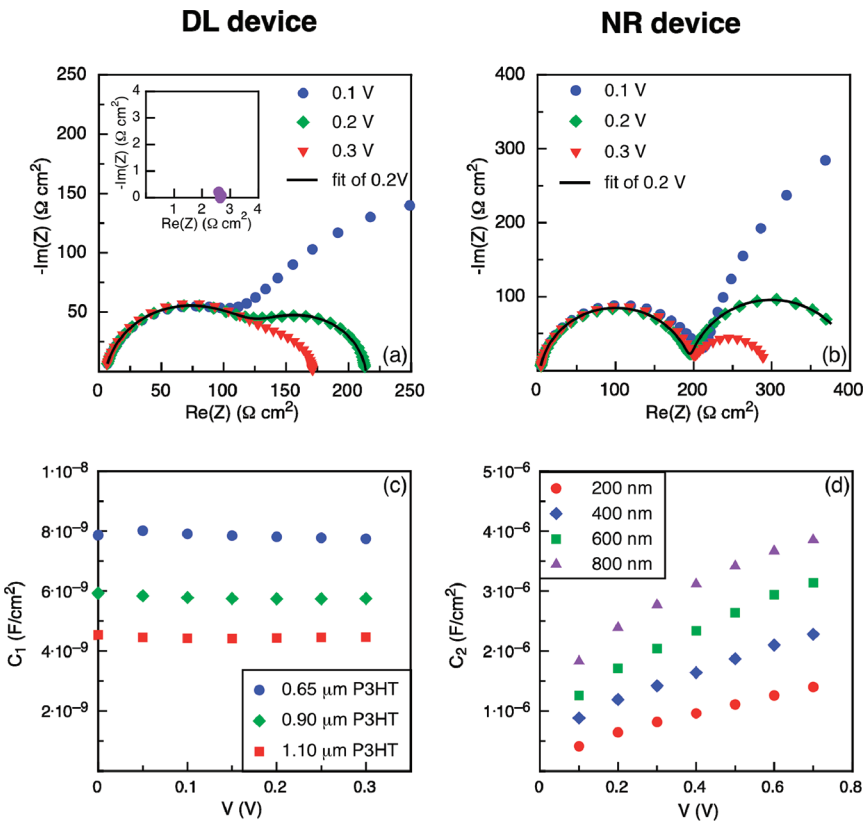

Figure 2. Experimental impedance spectra acquired at different bias voltages (full symbols) and corresponding fits (solid lines) of a DL device (a) and a NR device (b) applying the impedimetric model introduced in Figure 1. The inset to (a) shows the spectrum of a dense ZnO layer sandwiched between two electrodes (i.e., without polymer). (c) Extracted capacitance C_1 associated with the left semicircle for different layer thicknesses of the P3HT interlayer. (d) Capacitance C_2 associated with the right semicircle in the impedance spectra for different nanorod lengths.

often >0.95, thus implying that deviations from a perfect capacitive behavior are negligible.

The first step toward the identification of individual circuit elements is achieved by analyzing a device with a ZnO dense layer but missing polymer interlayer (see inset to Figure 2a). In this case, a purely ohmic behavior can be recognized with a resistance of nearly 3 Ω cm^2, a value that agrees well with the serial resistance R_3 required to describe a DL device with P3HT interlayer (3 ± 1.5 Ω cm^2). Thus, R_3 can be assigned to the combined effect of all contributing parts with high charge carrier density and mobility (Ag top electrode, ITO base electrode, ZnO dense layer). To access the origin of the left semicircle in Figure 2a, the thickness of the P3HT interlayer has systematically been varied from 0.65 to 1.1 μm. Figure 2c summarizes the extracted values of C_1 as a function of bias voltage for the different P3HT thicknesses. While C_1 is found to be independent of the applied bias voltage, a noticeable decrease in capacitance is observed with increasing polymer layer thickness d. This decrease in capacitance scales well with $1/d$, thereby identifying the P3HT film as a dielectric layer in a simple parallel plate capacitor. This picture is also confirmed by the corresponding R_1 value, which is found to be directly proportional to the polymer thickness d. Consequently, the remaining elements in our impedimetric model, C_2 and R_2, are related to the right-side semicircle, which can be assigned to the remaining ZnO/P3HT (semiconductor/semiconductor) interface, i.e., that part of our solar cell which is in the focus of interest here.

Turning our attention now to the NR devices, the more complex setup of the nanostructured solar cells surprisingly does not induce any additional spectral features, as can be recognized in Figure 2b. As before, the spectra reveal two semicircles, with the left-sided one (representing R_1 and C_1) again being independent of the applied bias voltage but shifted by a small offset on the real axis (representing R_3), and the right-sided one being strongly bias-dependent (R_2, C_2). Because the latter reflects the properties of the ZnO/P3HT interface, a sequence of nanostructured samples was studied to unravel the correlation between (R_2, C_2) and the length of the ZnO nanorods. Figure 2d displays the extracted C_2 value as a function of bias voltage for the different lengths. Obviously, an increased interface capacitance is induced for rising nanorod length, which indeed can be expected due to an enlarged ZnO/P3HT interfacial area. The strong dependence of C_2 on the bias voltage furthermore agrees well with observations reported earlier for donor−acceptor interfaces of several kinds of solar cells.[34,38,46] Longer nanorods also provide a larger interface area for charge carriers to travel through, which is expressed in a reduction of the extracted R_2 value with increasing rod length (not shown here). These results confirm the proper impedimetric description of the ZnO/P3HT interface by means of an (R, C) combination, which is also supported from a theoretical point of view.[33] Consequently, impedimetric parameters can be used as valuable tools to study changes in photovoltaic efficiency upon specific sample treatments as described in the following.

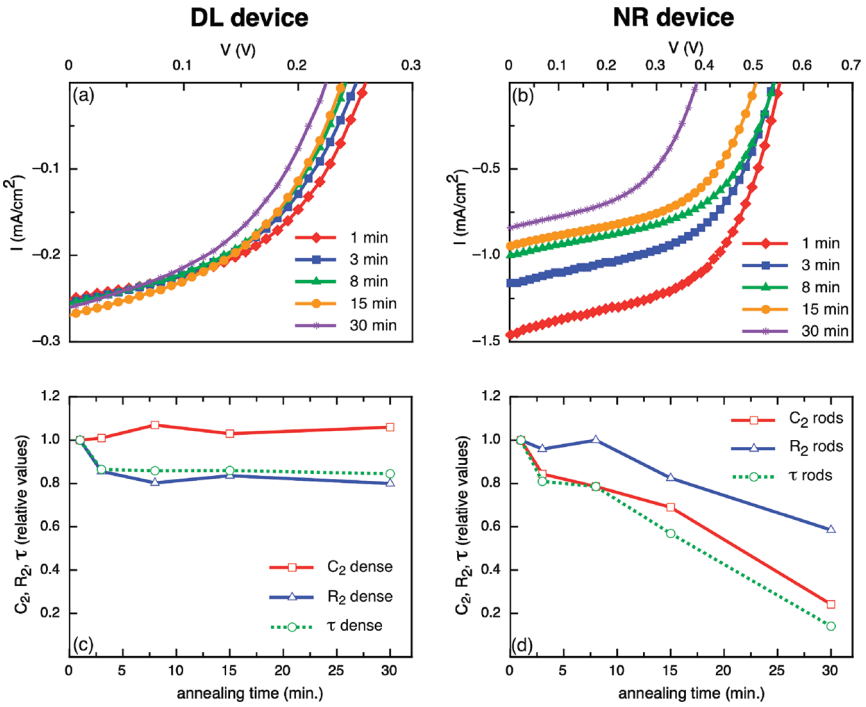

Figure 3. $I-V$ curves of DL (a) and NR (b) devices that were annealed for different times during fabrication. (c) and (d) show C_2, R_2, and corresponding τ (at V_{oc}) for the devices presented in (a) and (b), respectively.

A series of DL and NR solar cells were prepared for which the melting time of the P3HT during device fabrication was varied from 1 to 30 min. Panels a and b of Figure 3 show current−voltage ($I-V$) curves for both series of devices as a function of P3HT melting time. Clearly, a striking difference between both architectures can be observed: while the efficiency of the DL devices is found to dependent only weakly on the time the polymer has been in the molten state, in case of the NR devices, the short-circuit current and the open-circuit voltage both collapse upon annealing. To better understand the underlying changes in sample morphology, all annealing steps were monitored by impedimetric characterization as well. When the corresponding spectra are analyzed using the impedimetric model as described before, important conclusions can be drawn from the extracted parameters: (i) R_1 and C_1 representing the dielectric properties of the polymer do not depend on melting time for either the DL or the NR devices. This behavior is consistent with the ability of P3HT to withstand prolonged melting times, with no change in the level of crystallinity.[17] Additional XPS measurements performed to verify the chemical state of P3HT after such heat treatments furthermore did not show any hint for degradation effects like, e.g., the oxidation of the involved sulfur atoms, thereby indicating a high chemical stability of the polymer during melting as well. (ii) The values of R_2 and C_2 representing the ZnO/P3HT interface, together with the associated time constant τ (=RC), derived at a bias voltage corresponding to the open-circuit voltage, show subtle differences between the two device architectures. This is demonstrated in Figure 3c,d where, for DL devices, the relative values of R_2 and C_2 remain roughly constant for extended annealing times. This results in a fairly constant value of τ that nicely correlates to a nearly constant photovoltaic efficiency, as seen in Figure 3a. In contrast, in the case of the NR devices (Figure 3d), the extracted parameters R_2 and C_2 (and thus τ) are clearly decreasing, which also correlates to a reduction in efficiency with increasing annealing time (Figure 3b).

Because τ can be taken as a measure for recombination processes occurring at the donor−acceptor (P3HT/ZnO) interface, a decreasing value of τ suggests that the thermal treatment considerably promotes recombination in NR devices (lower τ means higher recombination rates) whereas in DL devices it has almost no effect.[33] Because DL and NR devices only differ in the interfacial area between ZnO and P3HT, the pronounced decrease of τ observed for NR devices should be related to subtle differences in their interface morphology. While a nanocrystalline dense layer of ZnO (as used for the DL devices) consists of adjacent grains with a large distribution of crystal directions, the nanorod array is characterized by single-crystalline pillars which are all (nearly) perfectly oriented in the [002] direction (see Supporting Information). Consequently, in the former case, the morphology of the P3HT near the ZnO will reflect the statistical distribution of crystal directions of the grains, and in the latter case, the P3HT will attach to the [100]-type surfaces of the ZnO rods in the same manner all over the entire interface area (i.e., polymer backbone perpendicular to nanorods).[43] Therefore, according to the sketch depicted in Figure 1, for NR devices, the polymer strands in contact with the ZnO surface basically orient into the horizontal direction with superior electrical conduction along individual chains (i.e., in horizontal direction), but significantly reduced conduction in the normal direction because this requires hopping of holes between neighboring chains after exciton splitting. This interpretation explains the decrease in photovoltaic efficiency with annealing time as being due to a reduced hole conduction toward the top electrode in the vicinity of the nanorod surfaces (where the excitons are split), resulting in an increased recombination rate (reduced lifetime) of holes that are localized on individual chains and that are able to easily

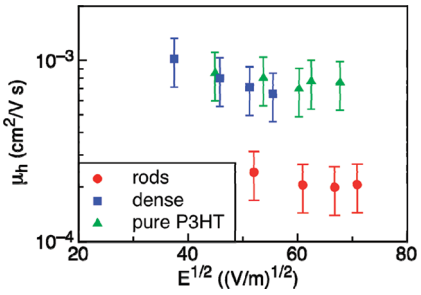

Figure 4. Hole mobility as a function of electric field for pure P3HT (sandwiched between ITO and Ag electrodes), for a DL device, and for a NR device.

move back toward the (negatively charged) nanorods. Further support for such a picture arises from the observed trends in R_2. The more time the polymer strands are provided to attach perpendicularly onto the nanorods during melting, the higher the number of pathways across the interface will be, thus explaining the decreasing value of R_2. Unfortunately, the drop in interface capacitance C_2 can hardly be explained without an appropriate theoretical treatment. On the other hand, for DL devices, the modification of interface properties as a consequence of changing P3HT morphology is much weaker, as only a small fraction of the interface area shares the same [100] direction and, thus, the resulting preferential P3HT morphology.

To further support the conclusions drawn above, additional measurements were performed, aiming to access the hole mobility μ_h of the P3HT for the different device configurations. Charge extraction in a linearly increasing voltage (CELIV) measurements were carried out by ramping a voltage (applied to the outer electrodes), thereby probing both the bulk and the interfacial polymer, respectively. Figure 4 summarizes the μ_h values acquired on three different samples: a pure P3HT layer sandwiched between ITO and Ag electrodes, a DL device, and a NR device (all annealed for 30 min at 225 °C). Obviously, the mobilities of holes in pure P3HT and P3HT within a DL device are identical, implying that the presence of a dense ZnO layer does not cause a change in the polymer's electrical properties. In contrast, μ_h in the case of the NR device drops severely by a factor of 4, evidencing that the origin of the reduced mobility lies exclusively in the presence of a significantly different interface (morphology), which hinders vertical transport of holes toward the top electrode, most likely due to the alignment of the polymer chains perpendicular to the ([100]-type) nanorod surfaces, as predicted earlier.[43] Although, at present, the results from the current work strongly support this latter premise, a final proof needs to be provided, requiring a detailed analysis of the phase morphology and reorganization of P3HT near the different ZnO facets.

CONCLUSION

In summary, an impedimetric model is proposed for the characterization of nanostructured ZnO/P3HT based solar cells, and its basic elements are successfully related to their physical origin. The comparison between ZnO dense layer (DL) and ZnO nanorod (NR) devices allows us to investigate the response of such hybrid solar cells to a heat treatment that is required for device fabrication. The efficiency of DL devices is almost independent of the melting time of the polymer, whereas in NR devices the efficiency decreases severely upon annealing. By localizing the impedimetric parameters representing the ZnO/P3HT interface, we can trace the origin of the degradation back as being likely due to the alignment of the polymer chains perpendicular to the [100] crystal direction of the ZnO nanorods, causing increased interfacial recombination of adjacent charge carriers.

Turning this argument around, the efficiency of nanostructured hybrid solar cells might significantly be improved in the future by precisely engineering the morphology of the polymer at the nanorod/polymer interface using self-organization strategies combined with suitable organic interlayers.

ASSOCIATED CONTENT

Supporting Information. Scanning electron microscopy images of a ZnO nanorod array; nanorod diameter distribution; XRD spectrum of a dense ZnO layer and a ZnO nanorod array. This material is available free of charge via the Internet at http://pubs.acs.org.

AUTHOR INFORMATION

Corresponding Author
*E-mail: bert.conings@uhasselt.be.

ACKNOWLEDGMENT

This work was financially supported by BOF (Hasselt University), the Flemish Odysseus program, and the Interreg project Organext. The authors are grateful for technical support by Johnny Baccus and Johan Soogen.

REFERENCES

(1) Halls, J. J. M.; Walsh, C. A.; Greenham, N. C.; Marseglia, E. A.; Friend, R. H.; Moratti, S. C.; Holmes, A. B. *Nature* **1995**, *376*, 498.
(2) Deibel, C.; Dyakonov, V. *Rep. Prog. Phys.* **2010**, 73.
(3) Dennler, G.; Scharber, M. C.; Brabec, C. J. *Adv. Mater.* **2009**, *21*, 1323.
(4) Thompson, B. C.; Fréchet, J. M. J. *Angew. Chem. Intl. Ed.* **2008**, *47*, 58.
(5) Oosterhout, S. D.; Wienk, M. M.; van Bavel, S. S.; Thiedmann, R.; Jan Anton Koster, L.; Gilot, J.; Loos, J.; Schmidt, V.; Janssen, R. A. J. *Nat. Mater.* **2009**, *8*, 818.
(6) Swinnen, A.; Haeldermans, I.; Vanlaeke, P.; D'Haen, J.; Poortmans, J.; D'Olieslaeger, M.; Manca, J. V. *Eur. Phys. J. Appl. Phys.* **2006**, *36*, 251.
(7) Campoy-Quiles, M.; Ferenczi, T.; Agostinelli, T.; Etchegoin, P. G.; Kim, Y.; Anthopoulos, T. D.; Stavrinou, P. N.; Bradley, D. D. C.; Nelson, J. *Nat. Mater.* **2008**, *7*, 158.
(8) Martens, T.; D'Haen, J.; Munters, T.; Beelen, Z.; Goris, L.; Manca, J.; D'Olieslaeger, M.; Vanderzande, D.; De Schepper, L.; Andriessen, R. *Synth. Met.* **2003**, *138*, 243.
(9) Bredas, J. L.; Norton, J. E.; Cornil, J.; Coropceanu, V. *Acc. Chem. Res.* **2009**, *42*, 1691.
(10) Lin, C.; Pan, W. C.; Tsai, F. Y. *Synth. Met.* **2010**, *160*, 2543.
(11) Park, H. Y.; Kim, K.; Kim, D. Y.; Choi, S. K.; Jo, S. M.; Jang, S. Y. *J. Mater. Chem.* **2011**, *21*, 4457.
(12) Saito, M.; Fujihara, S. *Energy Environ. Sci.* **2008**, *1*, 280.
(13) Ravirajan, P.; Peiro, A. M.; Nazeeruddin, M. K.; Grätzel, M.; Bradley, D. D. C.; Durrant, J. R.; Nelson, J. *J. Phys. Chem. B* **2006**, *110*, 7635.

(14) Peiro, A. M.; Ravirajan, P.; Govender, K.; Boyle, D. S.; O'Brien, P.; Bradley, D. D. C.; Nelson, J.; Durrant, J. R. *J. Mater. Chem.* **2006**, *16*, 2088.
(15) Olson, D. C.; Piris, J.; Collins, R. T.; Shaheen, S. E.; Ginley, D. S. *Thin Solid Films* **2006**, *496*, 26.
(16) Guo, M.; Diao, P.; Wang, X.; Cai, S. *J. Solid State Chem.* **2005**, *178*, 3210.
(17) Baeten, L.; Conings, B.; Boyen, H.-G.; D'Haen, J.; Hardy, A.; D'Olieslaeger, M.; Manca, J. V.; Van Bael, M. K. *Adv. Mater.* **2011**, *23*, 2802.
(18) Greene, L. E.; Law, M.; Goldberger, J.; Kim, F.; Johnson, J. C.; Zhang, Y.; Saykally, R. J.; Yang, P. *Angew. Chem. Int. Ed.* **2003**, *42*, 3031.
(19) Vayssieres, L. *Adv. Mater.* **2003**, *15*, 464.
(20) Law, M.; Greene, L. E.; Johnson, J. C.; Saykally, R.; Yang, P. *Nat. Mater.* **2005**, *4*, 455.
(21) Hara, K.; Horiguchi, T.; Kinoshita, T.; Sayama, K.; Sugihara, H.; Arakawa, H. *Sol. Energy Mater. Sol. Cells* **2000**, *64*, 115.
(22) Kislyuk, V. V.; Dimitriev, O. P. *J. Nanosci. Nanotechnol.* **2008**, *8*, 131.
(23) Heo, Y. W.; Norton, D. P.; Tien, L. C.; Kwon, Y.; Kang, B. S.; Ren, F.; Pearton, S. J.; LaRoche, J. R. *Mater. Sci. Eng., R* **2004**, *47*, 1.
(24) Baxter, J. B.; Aydil, E. S. *Sol. Energy Mater. Sol. Cells* **2006**, *90*, 607.
(25) Chen-Hao, K.; Jih-Jen, W. *Nanotechnology* **2007**, *18*, 505706.
(26) Monson, T. C.; Lloyd, M. T.; Olson, D. C.; Lee, Y.-J.; Hsu, J. W. P. *Adv. Mater.* **2008**, *20*, 4755.
(27) Wu, J.-J.; Chen, G.-R.; Yang, H.-H.; Ku, C.-H.; Lai, J.-Y. *Appl. Phys. Lett.* **2007**, *90*, 213109.
(28) Olson, D. C.; Lee, Y.-J.; White, M. S.; Kopidakis, N.; Shaheen, S. E.; Ginley, D. S.; Voigt, J. A.; Hsu, J. W. P. *J. Phys. Chem. C* **2007**, *111*, 16640.
(29) Lloyd, M. T.; Prasankumar, R. P.; Sinclair, M. B.; Mayer, A. C.; Olson, D. C.; Hsu, J. W. P. *J. Mater. Chem.* **2009**, *19*, 4609.
(30) Barsoukov, E.; Macdonald, J. R. *Impedance Spectroscopy - Theory, Experiment, and Applications*, 2nd ed.; John Wiley & Sons, Inc.: Hoboken, NJ, 2005.
(31) Bisquert, J. *J. Phys. Chem. B* **2001**, *106*, 325.
(32) Wu, S.; Li, J.; Tai, Q.; Yan, F. *J. Phys. Chem. C* **2010**, *114*, 21873.
(33) Bisquert, J.; Fabregat-Santiago, F.; Mora-Seró, I.; Garcia-Belmonte, G.; Giménez, S. *J. Phys. Chem. C* **2009**, *113*, 17278.
(34) Fabregat-Santiago, F.; Bisquert, J.; Palomares, E.; Otero, L.; Kuang, D.; Zakeeruddin, S. M.; Grätzel, M. *J. Phys. Chem. C* **2007**, *111*, 6550.
(35) Longo, C.; Nogueira, A. F.; De Paoli, M.-A.; Cachet, H. *J. Phys. Chem. B* **2002**, *106*, 5925.
(36) Wang, Q.; Ito, S.; Grätzel, M.; Fabregat-Santiago, F.; Mora-Seró, I.; Bisquert, J.; Bessho, T.; Imai, H. *J. Phys. Chem. B* **2006**, *110*, 25210.
(37) Garcia-Belmonte, G.; Munar, A.; Barea, E. M.; Bisquert, J.; Ugarte, I.; Pacios, R. *Org. Electron.* **2008**, *9*, 847.
(38) Wu, S.; Tai, Q.; Yan, F. *J. Phys. Chem. C* **2010**, *114*, 6197.
(39) Tai, Q.; Zhao, X.; Yan, F. *J. Mater. Chem.* **2010**, *20*, 7366.
(40) Bi, D.; Wu, F.; Yue, W.; Guo, Y.; Shen, W.; Peng, R.; Wu, H.; Wang, X.; Wang, M. *J. Phys. Chem. C* **2010**, *114*, 13846.
(41) Lee, Y.-J.; Lloyd, M. T.; Olson, D. C.; Grubbs, R. K.; Lu, P.; Davis, R. J.; Voigt, J. A.; Hsu, J. W. P. *J. Phys. Chem. C* **2009**, *113*, 15778.
(42) Mozer, A. J.; Sariciftci, N. S.; Lutsen, L.; Vanderzande, D.; Osterbacka, R.; Westerling, M.; Juska, G. *Appl. Phys. Lett.* **2005**, *86*, 112104.
(43) Dag, S.; Wang, L.-W. *Nano Lett.* **2008**, *8*, 4185.
(44) Wang, G.; Chen, D.; Zhang, H.; Zhang, J. Z.; Li, J. *J. Phys. Chem. C* **2008**, *112*, 8850.
(45) Tornow, J.; Schwarzburg, K. *J. Phys. Chem. C* **2007**, *111*, 8692.
(46) Garcia-Belmonte, G.; Boix, P. P.; Bisquert, J.; Sessolo, M.; Bolink, H. J. *Sol. Energy Mater. Sol. Cells* **2010**, *94*, 366.